Acta Mech. Sin. (2016) 32(1):135–143
DOI 10.1007/s10409-015-0499-1

RESEARCH PAPER

An anisotropic micromechanics model for predicting the rafting direction in Ni-based single crystal superalloys

Shuang-Yu Li[1] · **Wen-Ping Wu**[1,2] · **Ming-Xiang Chen**[1,2]

Received: 9 June 2015 / Revised: 19 July 2015 / Accepted: 20 August 2015 / Published online: 23 September 2015

Abstract An anisotropic micromechanics model based on the equivalent inclusion method is developed to investigate the rafting direction of Ni-based single crystal superalloys. The micromechanical model considers actual cubic structure and orthogonal anisotropy properties. The von Mises stress, elastic strain energy density, and hydrostatic pressure in different inclusions of micromechanical model are calculated when applying a tensile or compressive loading along the [001] direction. The calculated results can successfully predict the rafting direction for alloys exhibiting a positive or a negative mismatch, which are in agreement with pervious experimental and theoretical studies. Moreover, the elastic constant differences and mismatch degree of the matrix and precipitate phases and their influences on the rafting direction are carefully discussed.

Keywords Ni-based single crystal superalloys · Rafting · Equivalent inclusion theory · Stroh formalism

1 Introduction

Ni-based single crystal superalloys are used as indispensable materials for the blades and vane applications in gas turbines, owing to their excellent reliability and mechanical properties. They are strengthened by a high volume fraction of hard cubical γ' precipitates embedded coherently in a softer γ matrix. When superalloys are subjected to external stress at above 1123 K, the γ' precipitates coarsen directionally to form rafts generally aligned along the [001] direction. This rafting behavior directly affects the creep fatigue life of Ni-based single crystal superalloys and fracture surface is usually along the direction of rafting [1–3]. Therefore, the rafting mechanism is the key rule of precipitation hardening and mechanical properties in Ni-based single crystal superalloys.

The rafting of γ' precipitates under the influence of an applied stress was first studied in detail by Tien and Copley [4]. Subsequently, γ' rafting and its influence on the creep resistance of superalloys have been widely observed by experiments [2,5,6]. Moreover, some theoretical models based on dislocation [7,8], phase-field multi-component models incorporating elastic driving forces in the presence of a lattice misfit [9], crystal plasticity model taking into account microstructure evolutions [10], and numerical models in the framework of the finite element method [11–13] have been proposed to describe and predict the rafting behavior at high temperatures. These models have their own advantages for predicting the directional coarsening (rafting) and inelastic behaviors from a different point of view, mainly taking into account the influences of interfacial dislocations, microstructure evolutions, lattice mismatch, and the applied external stress, whereas they rarely consider the influence of the elastic constant differences of γ and γ', two phases on the rafting direction.

Furthermore, we have noticed that some micromechanical models based on Eshelby's equivalent inclusion theory have been successfully applied to describe the rafting, which occurs in the Ni-based single crystal superalloys. The isotropic elastic energy based on the theory of inclusion and

✉ Wen-Ping Wu
wpwu@whu.edu.cn

[1] Department of Engineering Mechanics, School of Civil Engineering, Wuhan University, Wuhan 430072, China

[2] State Key Laboratory of Water Resources & Hydropower Engineering Science, Wuhan University, Wuhan 430072, China

inhomogeneity by Eshelby was calculated and applied to predict correctly the γ' rafting [14,15]. Afterwards, Miyazaki et al. [16] and Ratel et al. [17] developed the inclusion theory with anisotropic elasticity to calculate elastic energy caused by the change in the shape of the γ' precipitates, and predicted effectively the directional coarsening of the γ' precipitates in the case of a creep stress applied along the [001] direction. Based on this model, Ratel et al. [18] further analyzed the effect of the plastic strain in the horizontal channels and vertical channels in the γ matrix on the γ' rafting. In these equivalent inclusion models, the γ' precipitates was taken as an ellipsoidal inclusion, however, the actual γ' precipitates with a cubic structure, and the volume fraction of γ' may reach as high as 70%. Due to the equivalent inclusion method, it is being limited to applications for a material system in which the inclusions exist with a low volume fraction in an isolated style [19,20]. A three-phase micromechanical model with consideration of the cubic structure and high volume fraction of γ' was developed by Wu et al. [21] to predict the directional coarsening direction in Ni-based single crystal superalloys. However, this micromechanical model does not consider the anisotropy of Ni-based single crystal superalloys. Thus, in the present paper, we aim at improving that model and developing an anisotropic micromechanics model based on Eshelby's equivalent inclusion theory to predict the γ' rafting direction. The anisotropic cubical γ' precipitates with a volume fraction of 70 % embedded in the γ matrix is taken into account in our model, which equates to the actual structure in the Ni-based single crystal superalloys. Moreover, the effects of the mismatch degree and the elastic constant differences on the rafting direction are carefully discussed.

This paper is organized as follows: First, in Sect. 2.1, we introduce the anisotropic equivalent inclusion model. In Sects. 2.2–2.3, the Eshelby's equivalent inclusion theory is applied to this model and the solution of the average Eshelby tensor is given. Next, according to the equivalent inclusion model in Sect. 2, the von Mises stress, elastic strain energy density and hydrostatic pressure in different inclusions are calculated when the external stress is applied along the [001] direction in Sect. 3. Meanwhile, the effects of the sign of mismatch (positive or negative) and the external load (tensile or compressive) on the rafting direction are analyzed. Then the effects of mismatch degree and elastic constant differences on von Mises stress are discussed in Sect. 4. Finally, some key conclusions are drawn in Sect. 5.

2 Model and method

2.1 Micromechanical model

The material micromechanical model and its representative volume element are shown in Fig. 1. As shown in Fig. 1a,

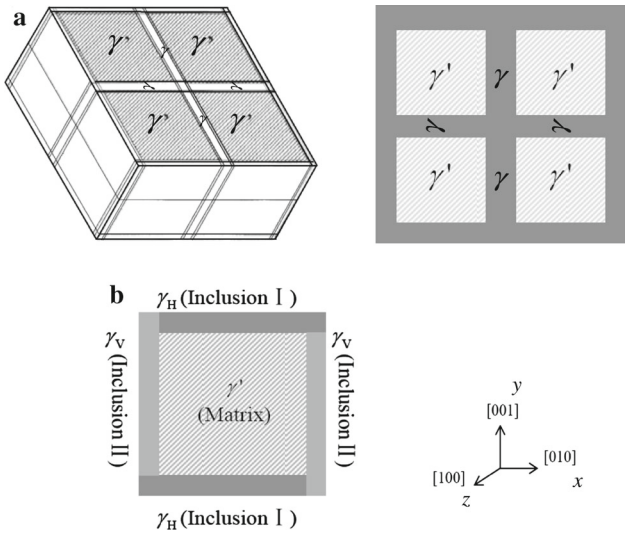

Fig. 1 Material model of Ni-based single crystal superalloys: the cubical γ' precipitates are uniformly embedded in the γ matrix and the volume fraction of the γ' phase is 70 % **a**, and the representative volume element for micromechanical analysis **b**

the γ' precipitates with the cubical shapes are uniformly distributed in the γ matrix and the volume fraction of the γ' precipitate is 70 %. Generally, the equivalent inclusion method is limited to application for a material system in which the inclusions exist with a low volume fraction in an isolated style. However, the current Ni-based single crystal superalloys contain γ' precipitates with a very high volume fraction. Based on our previous model [21], we take the γ' precipitates as the matrix and the γ matrix as the inclusions. In addition, the horizontal matrix γ_{H} and the vertical matrix γ_{V} are considered as the inclusion I and the inclusion II, respectively, as shown in Fig. 1b. Therefore, a three-phase composite material model is established in the selected representative volume element, consisting of the matrix, inclusion I and inclusion II.

In the present model, the elastic tensors of the matrix, inclusion I and inclusion II, are denoted by $\boldsymbol{C}, \boldsymbol{C}^1, \boldsymbol{C}^2$; the volume fractions by f, f_1, f_2 (with $f = 0.7$, $f_1 = f_2 = 0.15$), respectively. As in Zhou et al. [13], when the temperature is at 1323 and 1023 K, the elastic constants of the γ' precipitates and the γ matrix for negative and positive mismatch are listed in Table 1.

In the calculation, the coordinate system is identical to the crystal coordinate axes. Due to the material along the direction of [100] being uniform and in a periodic array, this model is simplified as a plane strain problem. As in Chen et al. [22], a thermal expansion method is used to realize the effect of lattice mismatch. The thermal mismatch strains can be given such that $\boldsymbol{\varepsilon}^{\mathrm{t}} = [-\delta, -\delta, 0, 0, 0, 0]^{\mathrm{T}}$, with superscript T denoting the transpose of the vector and δ denoting lattice mismatches.

Table 1 Elastic constants (in GPa) of γ matrix and γ' precipitates at 1323 and 1023 K for the negative mismatch $\delta = -0.38\,\%$ and positive mismatch $\delta = 0.56\,\%$, respectively

Material	δ (%)	C_{11}	C_{12}	C_{44}
γ matrix	−0.38	202	139	95
γ' precipitates	−0.38	179	120	88
γ matrix	0.56	112	63	57
γ' precipitates	0.56	167	107	99

2.2 Micromechanical method

According to Mori and Tanaka [20], the average stress σ_{ij}^r of the inclusions can be written as

$$\sigma_{ij}^r = \sigma_{ij}^0 + \overline{\sigma_{ij}} + \overline{\sigma_{ij}^r}, \quad r = 1, 2, \tag{1}$$

where σ_{ij}^0 is uniform external stress; $\overline{\sigma_{ij}}$ is an average stress disturbance in the matrix due to the existence of the inclusions; $\overline{\sigma_{ij}} + \overline{\sigma_{ij}^r}$ is an average stress disturbance in the inclusions; the superscript $r = 1$ and 2 represent inclusion I and inclusion II, respectively. Applying Hooke's law, the average stress σ_{ij}^r of the inclusions is

$$\sigma_{ij}^r = \sigma_{ij}^0 + \overline{\sigma_{ij}} + \overline{\sigma_{ij}^r} = C_{ijkl}^r \left(\varepsilon_{kl}^0 + \overline{\varepsilon_{kl}} + \overline{\varepsilon_{kl}^r} - \varepsilon_{kl}^{\mathrm{t}}\right), \tag{2}$$

where C_{ijkl}^r is the elastic stiffness tensor of the inclusions; $\overline{\varepsilon_{ij}}$ is average strain disturbance in the matrix due to the existence of the inclusions; $\overline{\varepsilon_{ij}} + \overline{\varepsilon_{ij}^r}$ is the average strain disturbance in the inclusions. According to Eshelby's equivalent inclusion theory, the right item of Eq. (2) can be written as

$$\begin{aligned} &C_{ijkl}^r \left(\varepsilon_{kl}^0 + \overline{\varepsilon_{kl}} + \overline{\varepsilon_{kl}^r} - \varepsilon_{kl}^t\right) \\ &\quad = C_{ijkl} \left(\varepsilon_{kl}^0 + \overline{\varepsilon_{kl}} + \overline{\varepsilon_{kl}^r} - \varepsilon_{kl}^t - \varepsilon_{kl}^{*r}\right), \end{aligned} \tag{3}$$

where C_{ijkl} is the elastic stiffness tensor of the matrix; ε_{ij}^{*r} is the fictitious eigenstrain. For the entire composite domain, the following relation always holds

$$\sigma_{ij}^0 = C_{ijkl}\varepsilon_{kl}^0. \tag{4}$$

To facilitate Eshelby's formula, we introduce ε_{ij}^{**r} defined by

$$\varepsilon_{ij}^{**r} = \varepsilon_{ij}^{\mathrm{t}} + \varepsilon_{ij}^{*r}. \tag{5}$$

Thus, according to Eqs. (2)–(5), we have

$$\overline{\sigma_{ij}^r} = C_{ijkl} \left(\overline{\varepsilon_{kl}^r} - \varepsilon_{kl}^{**r}\right). \tag{6}$$

The strain disturbance $\overline{\varepsilon_{ij}^r}$ is related to ε_{ij}^{**r} through an average Eshelby tensor $\overline{S_{ijkl}^r}$,

$$\overline{\varepsilon_{ij}^r} = \overline{S_{ijkl}^r}\varepsilon_{kl}^{**r}, \tag{7}$$

where the average Eshelby tensor of the inclusions $\overline{S_{ijkl}^r}$ is shown in Sect. 2.3.

Substitution of Eqs. (4)–(7) into Eq. (3) yields the equivalent eigenstrain ε_{ij}^{**r}

$$\begin{aligned} \varepsilon_{ij}^{**r} = &\left(\Delta C_{ijkl}^r \overline{S_{klmn}^r} + C_{ijmn}\right)^{-1} \\ &\times \left[-\Delta C_{mnpq}^r \left(\varepsilon_{pq}^0 + \overline{\varepsilon_{pq}}\right) + C_{mnpq}^r \varepsilon_{pq}^{\mathrm{t}}\right], \end{aligned} \tag{8}$$

where $\Delta C_{ijkl}^r = C_{ijkl}^r - C_{ijkl}$ and $C_{ijkl}^1 = C_{ijkl}^2$. Due to the vanishing of the average stress disturbance over the entire composite domain, $\overline{\varepsilon_{ij}}$ is determined by

$$\overline{\varepsilon_{ij}} + \sum_{r=1}^{2} f_r \left(\overline{\varepsilon_{ij}^r} - \varepsilon_{ij}^{**r}\right) = 0. \tag{9}$$

Substituting Eq. (7) into Eq. (9), we have

$$\overline{\varepsilon_{ij}} = -\sum_{r=1}^{2} f_r \left(\overline{S_{ijkl}^r} - I_{ijkl}\right) \varepsilon_{kl}^{**r}, \tag{10}$$

where I_{ijkl} is a fourth order unity tensor. Substitution of Eq. (8) into Eq. (10) gives

$$\begin{aligned} \overline{\varepsilon_{ij}} = &-\sum_{r=1}^{2} f_r \left(\overline{S_{ijkl}^r} - I_{ijkl}\right) \left(\Delta C_{klmn}^r \overline{S_{mnpq}^r} + C_{klpq}\right)^{-1} \\ &\times \left[-\Delta C_{pqgh}^r \left(\varepsilon_{gh}^0 + \overline{\varepsilon_{gh}}\right) + C_{pqgh}^r \varepsilon_{gh}^{\mathrm{t}}\right]. \end{aligned} \tag{11}$$

It can be simplified to

$$\overline{\varepsilon_{ij}} = \left(I_{ijkl} - U_{ijkl}\right)^{-1} \left(U_{klmn}\varepsilon_{mn}^0 - V_{klmn}\varepsilon_{mn}^{\mathrm{t}}\right), \tag{12}$$

where

$$\begin{aligned} U_{ijkl} = &\sum_{r=1}^{2} f_r \left(\overline{S_{ijmn}^r} - I_{ijmn}\right) \\ &\times \left(\Delta C_{mnpq}^r \overline{S_{pqgh}^r} + C_{mngh}\right)^{-1} \Delta C_{ghkl}^r, \end{aligned} \tag{13}$$

$$\begin{aligned} V_{ijkl} = &\sum_{r=1}^{2} f_r \left(\overline{S_{ijmn}^r} - I_{ijmn}\right) \\ &\times \left(\Delta C_{mnpq}^r \overline{S_{pqgh}^r} + C_{mngh}\right)^{-1} C_{ghkl}^r. \end{aligned} \tag{14}$$

According to Eqs. (2)–(5), and (7), the average stresses σ_{ij}^{r} inside the inclusions can be obtained as

$$\sigma_{ij}^{r} = \sigma_{ij}^{0} + C_{ijkl}\overline{\varepsilon_{kl}} + C_{ijkl}\left(\overline{S_{klmn}^{r}} - I_{klmn}\right)\varepsilon_{mn}^{**r}. \tag{15}$$

According to Eq. (4) and Eqs. (12)–(14), if the elastic constants of material, thermal mismatch strains $\varepsilon_{ij}^{\mathrm{t}}$, external stress σ_{ij}^{0}, and the average Eshelby tensor $\overline{S_{ijkl}^{r}}$ are given, we can obtain $\overline{\varepsilon_{ij}}$. Then substitution of Eq. (12) into Eq. (8) gives the new fictitious eigenstrain ε_{ij}^{**r}. Finally, according to Eq. (15), we can obtain the average stresses σ_{ij}^{r} inside the inclusions.

After the application of the Eshelby–Mori-Tanaka's theory, the von Mises stress σ_{e}^{r} is obtained by

$$\sigma_{\mathrm{e}}^{r} = \sqrt{\frac{3}{2}\left(s_{ij}^{r}s_{ij}^{r}\right)}, \quad s_{ij}^{r} = \sigma_{ij}^{r} - \frac{1}{3}\sigma_{kk}^{r}\delta_{ij}, \tag{16}$$

where s_{ij}^{r} is the stress deviator and δ_{ij} is Kronecker delta.

The elastic strain energy density G^{r} is given by

$$G^{r} = \frac{1}{2}\sigma_{ij}^{r}\varepsilon_{ij}^{r}. \tag{17}$$

The hydrostatic pressure σ_{h}^{r} is given by

$$\sigma_{\mathrm{h}}^{r} = \frac{1}{3}\sigma_{kk}^{r}. \tag{18}$$

Generally, for an anisotropic material, an equivalent stress based on Hill's yield criterion is more suitable to estimate whether the yielding occurs. However, in the present paper, the rafting direction of Ni-based single crystal superalloys is analyzed and predicted only in the elastic range. Therefore, the von Mises stress, elastic strain energy density, and hydrostatic pressure are calculated to predict the rafting direction as proposed in Zhou et al. [13].

According to these three mechanical variables, it should be noted that the initiation of rafting and its direction in Ni-based single crystal superalloys can be analyzed and conclusions made.

2.3 Average Eshelby tensor

When an inclusion Ω with uniform eigenstrain ε_{ij}^{**} is embedded in a two-dimensional infinitely extended homogeneous material, which has an elastic constant tensor of C_{ijkl} , the displacement $u_k(\boldsymbol{X})$ at the position $\boldsymbol{X}$ in the material is given by the elastic Green functions $u_j^k(\boldsymbol{x};\boldsymbol{X})$ as in Mura [23]

$$u_k(\boldsymbol{X}) = C_{ijlm}\varepsilon_{lm}^{**}\int_{\partial\Omega} u_j^k(\boldsymbol{x};\boldsymbol{X})\, n_i(\boldsymbol{x})\,\mathrm{d}S(\boldsymbol{x}), \tag{19}$$

where $\partial\Omega$ is the surface of Ω and $n_i(\boldsymbol{x})$ is the unit outward normal vector at $\boldsymbol{x}$ on the boundary $\partial\Omega$.

Substituting Eq. (19) into the formula of strain $\varepsilon_{ij} = \frac{1}{2}\left(u_{i,j} + u_{j,i}\right)$, we have

$$\varepsilon_{kp}(\boldsymbol{X}) = \frac{1}{2}C_{ijlm}\varepsilon_{lm}^{**}\int_{\partial\Omega} \times\left[u_{j,X_p}^{k}(\boldsymbol{x};\boldsymbol{X}) + u_{j,X_k}^{p}(\boldsymbol{x};\boldsymbol{X})\right] n_i(\boldsymbol{x})\,\mathrm{d}S(\boldsymbol{x}). \tag{20}$$

If the region of Ω is non-elliptic, the strain ε_{ij} in Ω due to the uniform eigenstrain ε_{ij}^{**} is not uniform as in Onaka et al. [24]. The average strain $\overline{\varepsilon_{ij}}$ in Ω is expressed as

$$\overline{\varepsilon_{ij}} = \frac{1}{A}\int_{\Omega}\varepsilon_{ij}(\boldsymbol{X})\,\mathrm{d}A(\boldsymbol{X}), \tag{21}$$

where A is the area of region Ω.

The average Eshelby tensor $\overline{S_{ijkl}}$ can be defined from $\overline{\varepsilon_{ij}}$ and ε_{ij}^{**} as

$$\overline{\varepsilon_{ij}} = \overline{S_{ijkl}}\varepsilon_{kl}^{**}. \tag{22}$$

According to Eqs. (19)–(22), if the expressions of Green's functions $u_j^k(\boldsymbol{x};\boldsymbol{X})$ are given, we can obtain the average Eshelby tensor $\overline{S_{ijkl}}$.

As in Pan [25], the two-dimensional Green functions $u_j^k(\boldsymbol{x};\boldsymbol{X})$ are expressed as

$$u_j^k(\boldsymbol{x};\boldsymbol{X}) = \frac{1}{\pi}\mathrm{Im}\left\{\sum_{r=1}^{3} A_{jr}A_{kr}\ln(z_r - s_r)\right\}, \tag{23}$$

where Im stands for the imaginary part of a complex number; the complex z_r and s_r are defined, respectively, by $z_r = x + p_r y$ and $s_r = X + p_r Y$; $\boldsymbol{A} = [\boldsymbol{a}_1, \boldsymbol{a}_2, \boldsymbol{a}_3]$, p_r and $\boldsymbol{a}_r$ denote the Stroh eigenvalues and eigenvectors with their expressions given in Appendix 1.

According to Pan [25], for the integral of Eq. (20), if the inclusion is rectangular, the contribution of each straight-line segment along the boundary of the inclusion can be obtained. The expressions are given in Appendix 2.

3 Model calculated results

3.1 Rafting direction at different signs of mismatch (positive or negative)

Figure 2 shows the variation of the von Mises stress, elastic strain energy density and hydrostatic pressure in the inclusions with external tensile stress along the [001] direction.

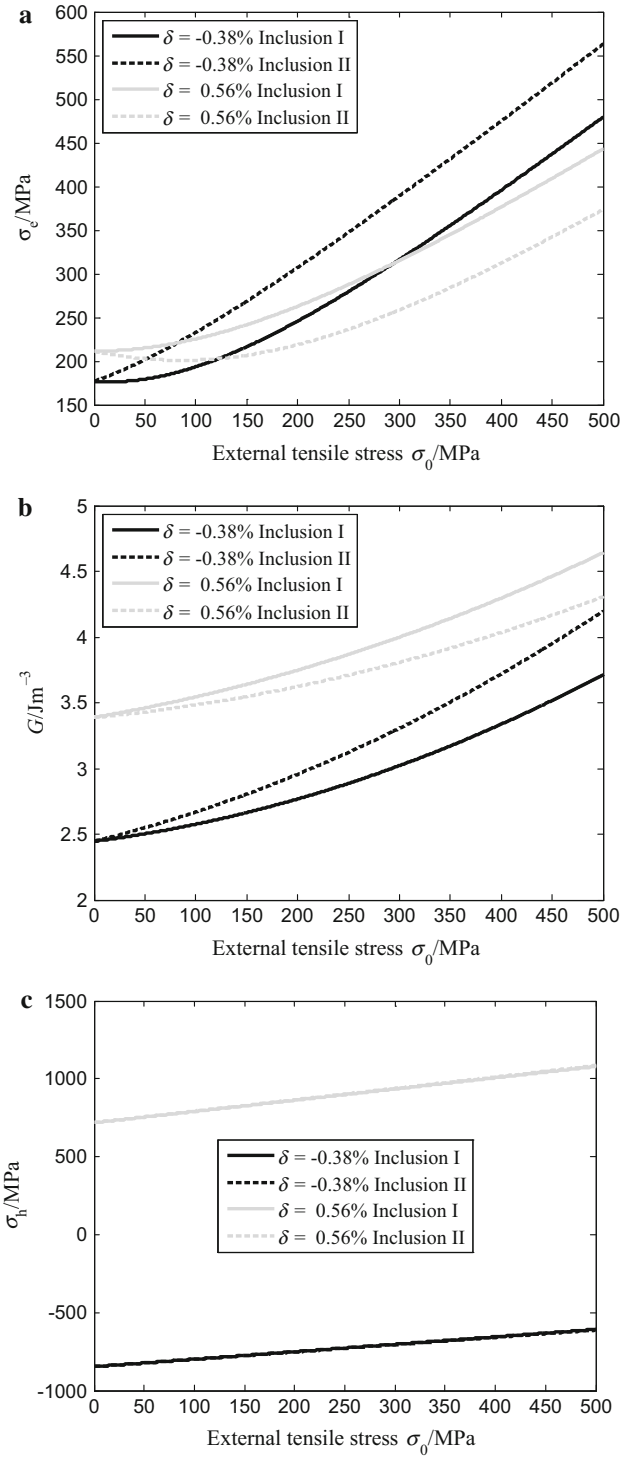

Fig. 2 The variation of the von Mises stress **a**, elastic strain energy density **b** and hydrostatic pressure **c** in the inclusions with the external tensile stress along the [001] direction

In the calculation, two kinds of mismatch $\delta = -0.38\,\%$ and $\delta = 0.56\,\%$ are selected. When the external stress is zero, we can find clearly in Fig. 2 that all these three values in the inclusion I equals the inclusion II for both the negative and positive mismatch cases. But the values of the von Mises stress and elastic strain energy density with a positive mismatch ($\delta = 0.56\,\%$) are larger than those with a negative mismatch ($\delta = -0.38\,\%$). The hydrostatic pressure is tensile stress within the inclusions for an alloy with a positive mismatch ($\delta = 0.56\,\%$), while the hydrostatic pressure is compressive stress within the inclusions with a negative mismatch ($\delta = -0.38\,\%$).

When a tensile stress is applied to a negative mismatch alloy ($\delta = -0.38\,\%$) along the [001] direction, as seen in Fig. 2a and b the von Mises stress, elastic strain energy density in the inclusion II are larger than those in the inclusion I, and the values of the von Mises stress and elastic strain energy density in the inclusions I and II increases with an external tensile stress increase. In Fig. 2c, the hydrostatic pressure increases with an external tensile stress increase, but the values of the hydrostatic pressure in the inclusion I and inclusion II are basically the same. On the other hand, when a tensile stress is applied to a positive mismatch alloy ($\delta = 0.56\,\%$) along the [001] direction, the situation is reversed.

Due to the higher von Mises stress and elastic strain energy density in the inclusion II for a negative mismatch alloy ($\delta = -0.38\,\%$), the inclusion II will preferentially occur as a plastic deformation, which induces the mixed dislocations generation and distribution predominantly in that region. The rafting direction is vertical to the [001] stress axes (horizontal matrix channel). In contrast, when a tensile stress is applied to an alloy with a positive mismatch ($\delta = 0.56\,\%$), the inclusion I will preferentially occur as a plastic deformation. The rafting direction is parallel to the [001] stress axes (vertical matrix channel). Furthermore, it seems difficult to determine the rafting direction using the hydrostatic pressure because their values in the inclusions I and II are basically the same. Therefore, comparing it to the calculation of hydrostatic pressure, it is easier to predict the rafting direction by calculating the von Mises stress and elastic strain energy density in different inclusions (matrix channels) of this model.

In addition, it is also noticeable that the von Mises stress in the inclusion II of the alloy with a positive mismatch decreases firstly with the increase of external stress, and then it increases. This is because the deformation, which is caused by the positive mismatch, is opposite to the deformation under the tensile stress along the [001] direction in the inclusion II.

3.2 Rafting direction at different external stress (tensile or compressive)

Figure 3 shows the variations of the von Mises stress, elastic strain energy density and hydrostatic pressure when an external tensile or compressive stress is applied to a negative mismatch alloy ($\delta = -0.38\,\%$) along the [001] direction. In Fig. 3a, b, we can find that the application of an external stress (tensile or compressive) leads to different values of the

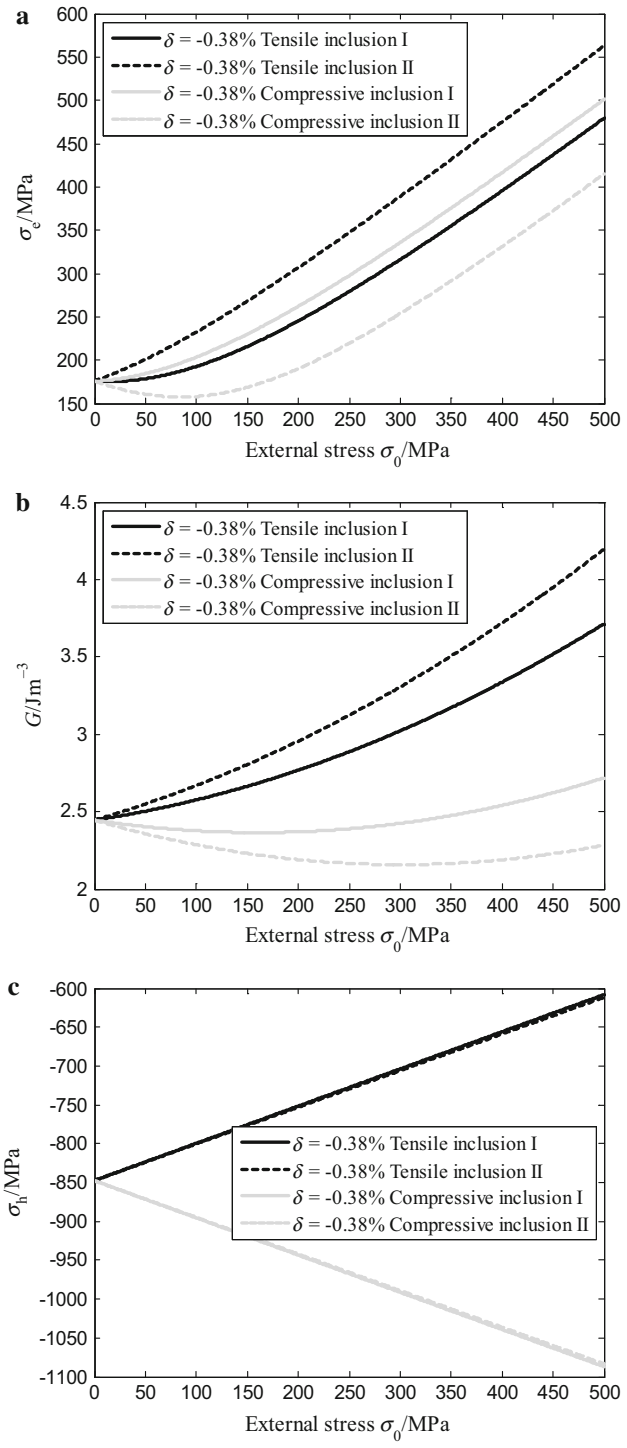

Fig. 3 The variation of the von Mises stress **a**, elastic strain energy density **b** and hydrostatic pressure **c** in the inclusions with external stress (tensile and compressive) for negative mismatch alloy ($\delta = -0.38\,\%$)

von Mises stress and elastic strain energy density both in the inclusion I and inclusion II. In Sect. 3.1, we have discussed the case that a tensile stress is applied to a negative mismatch alloy along the [001] direction. However, when a compressive stress is applied, the situation is reversed. The von Mises stress and elastic strain energy density in the inclusion I are larger than those in the inclusion II when a compressive stress is applied. As shown in Fig. 3c, the hydrostatic pressures of the inclusion I and inclusion II both decrease with the external compressive stress increasing, but there is still very little difference in the values of the hydrostatic pressure of the inclusions I and II.

Based on the above results, we can conclude that when an external tensile stress is applied to a negative mismatch superalloy along the [001] direction, due to the higher von Mises stress and elastic strain energy density in the inclusion II, plastic deformation will predominantly occur in the inclusion II. The rafting direction is vertical to the [001] stress axes (horizontal matrix channel). However, when a compressive stress is applied, plastic deformation will predominantly occur in the inclusion I, and the rafting direction is parallel to [001] stress axes (vertical matrix channel). These results are in good agreement with the previous experimental observations [2,4–6] and theoretical studies [7,8,14].

4 Discussion

4.1 The effect of mismatch degree on von Mises stress

For a negative mismatch alloy, the elastic constants (in Table 1) are fixed and the mismatch degree is changed from -0.8 % to 0.8 %. The variations of the von Mises stress in the inclusion I and inclusion II are shown in Fig. 4.

We can see from Fig. 4 that the von Mises stresses in the inclusions are closely related to mismatch degree. In Fig. 4a, when a tensile stress is applied to a negative mismatch alloy along the [001] direction, the von Mises stress in the inclusion II is larger than in the inclusion I, thus the rafting direction is vertical to the [001] stress axes (horizontal matrix channel) based on the analysis of Sect. 3. The von Mises stresses both in the inclusion I and inclusion II decrease with the increasing mismatch degree. While the mismatch degree is about 0, the von Mises stresses are the same in the inclusion I and inclusion II. However, when the mismatch is positive, the von Mises stress in the inclusion I is larger than in the inclusion II, and the rafting direction is parallel to the [001] stress axes (vertical matrix channel). Therefore, for a tensile stress applied along the [001] direction, the rafting direction also changed from a horizontal to a vertical matrix channel when the mismatch degree changed from negative to positive. By contrast, when a compressive stress is applied along the [001] direction, the results are reversed as shown in Fig. 4b.

4.2 The effect of elastic constant differences on von Mises stress

Figure 5 shows the effect of elastic constant differences on the von Mises stress. For a positive mismatch alloy ($\delta = 0.56\,\%$),

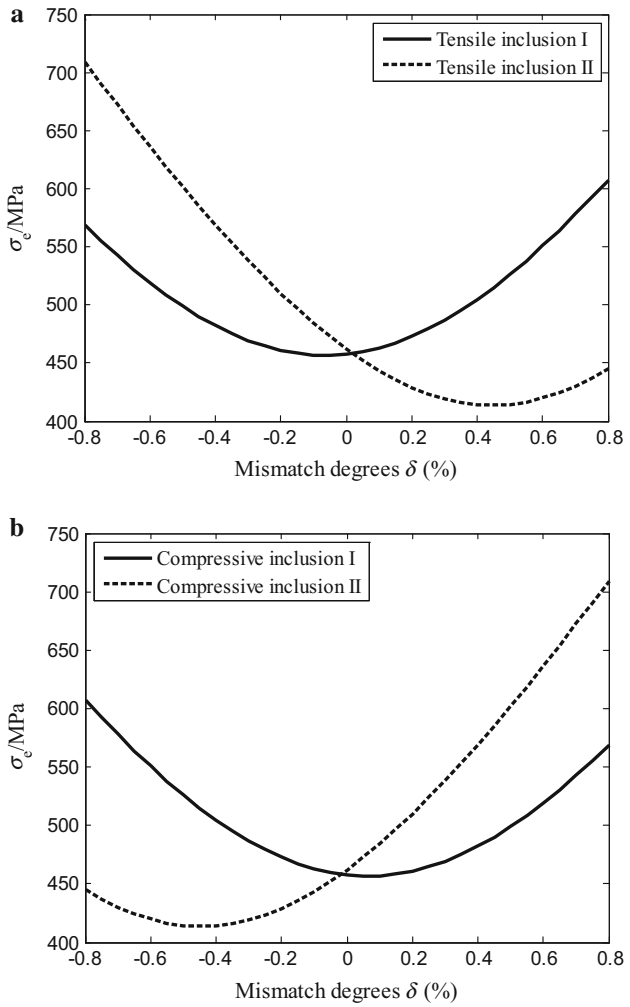

Fig. 4 The variation of the von Mises stress in the inclusions with different mismatch degrees under 500 MPa external tensile stress **a** or compressive stress **b**

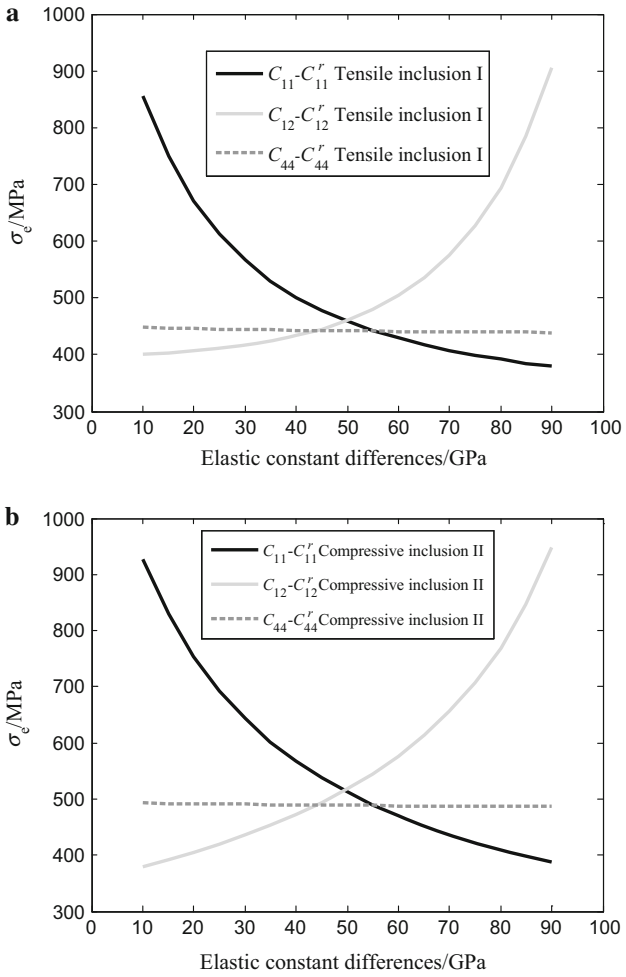

Fig. 5 The variations of the von Mises stress with different elastic constant differences in the inclusion I under 500 MPa external tensile stress **a** and in the inclusion II under 500 MPa external compressive stress

we change the three elastic constants of the γ' precipitates respectively (including C_{11}, C_{12}, C_{44}), and apply 500MPa external stress along the [001] direction. According to Sect. 3, when an external stress is tensile along the [001] direction, the von Mises stress of inclusion I is larger than inclusion II. Therefore, we only consider the effect of elastic constant differences between γ' phase and γ phase on the von Mises stress of inclusion I. The results are shown in Fig. 5a. When the first component $(C_{11} - C^r_{11})$ of the elastic constant differences between γ' phase and γ phase increases, the von Mises stress of inclusion I decreases; when the second component $(C_{12} - C^r_{12})$ of elastic constant differences between γ' phase and γ phase increases, the von Mises stress of inclusion I increases; however, while the third component $(C_{44} - C^r_{44})$ of elastic constant differences between γ' phase and γ phase increases, the von Mises stress of inclusion I does not display obvious variation. Thus, it indicates that the elastic constant difference $C_{44} - C^r_{44}$ has no significant effect on the von Mises stress, namely, it has no effect on the rafting direction of alloys.

Similarly, when the external stress is compressive along the [001] direction, according to Sect. 3, the von Mises stress of inclusion II is larger than inclusion I. Therefore, we only consider the effect of elastic constant differences between the γ' phase and γ phase on the von Mises stress of inclusion II. As shown in Fig. 5b, the results are the same as the case of the external tensile stress.

From the above discussion, the mismatch degree and elastic constant differences ($C_{11} - C^r_{11}$ and $C_{12} - C^r_{12}$) have a strong effect on the von Mises stress, the variant of $C_{44} - C^r_{44}$ has no effect on the von Mises stress. Due to the change of the elastic constant differences and mismatch degree leading to different values of the von Mises stress in the inclusion I and inclusion II, they cause the directional coarsening (rafting) in Ni-based single crystal superalloys.

5 Conclusions

A new anisotropic micromechanics model based on the equivalent inclusion method has been developed to predict the rafting direction in Ni-based single crystal superalloys. The anisotropic cubical γ' precipitate with a volume fraction of 70 % embedded in the γ matrix is taken into account in this model, which equates to the actual structure in the Ni-based single crystal superalloys. The von Mises stress, elastic strain energy density, and hydrostatic pressure of the inclusions (matrix of original material) are calculated when the external stresses are applied along the [001] direction. The main conclusions are as follows:

(1) The proposed anisotropic micromechanics model effectively predicts a rafting direction of Ni-based single crystal superalloys. The rafting direction depends on the sign of the mismatch (positive or negative) and the type of external stress (tensile or compressive). When a tensile stress is applied to an alloy with a positive mismatch or a compressive stress is applied to an alloy with a negative mismatch, the rafting direction is parallel to the [001] stress axes (vertical matrix channel). When a compressive stress is applied to an alloy with a positive mismatch or a tensile stress is applied to an alloy with a negative mismatch, the rafting direction is vertical to the [001] stress axes (horizontal matrix channel). These results agree well with previous theoretical predictions and experimental observations.
(2) The variations of mismatch degree and elastic constant differences play an important role on the von Mises stress of the γ matrix, which strongly affect the γ' rafting direction. When mismatch degree changes from a negative value to a positive value, the von Mises stress decreases first and then increases no matter how external stress is applied (tensile or compressive).
(3) The three different elastic constant differences have different influences on the von Mises stress (rafting direction). The elastic constant differences ($C_{11} - C_{11}^r$ and $C_{12} - C_{12}^r$) have a strong effect on the von Mises stress (rafting direction), but the variant of $C_{44} - C_{44}^r$ has almost no effect on the von Mises stress (rafting direction).

From the current results, it is clear to see the influence of some micromechanical parameters (including mismatch degree and elastic constant differences) on the von Mises stress in different inclusions. In comparison with finite element method used by Zhou et al. [13], this micromechanical model is more beneficial for achieving the transformation between macroscopic and mesoscopic physical quantities and reveals the relation among different physical quantities by considering mesoscopic structure and properties of materials.

Acknowledgments The work was supported by The National Natural Science Foundation of China (Grants 11102139 and 11472195), and The Natural Science Foundation of Hubei Province of China (Grant 2014CFB713).

Appendix 1

For anisotropic materials, the elastic constants matrix is symmetric and can be expressed as

$$\boldsymbol{C} = \begin{bmatrix} C_{11} & C_{12} & C_{13} & C_{14} & C_{15} & C_{16} \\ & C_{22} & C_{23} & C_{24} & C_{25} & C_{26} \\ & & C_{33} & C_{34} & C_{35} & C_{36} \\ & & & C_{44} & C_{45} & C_{46} \\ & \text{Sym.} & & & C_{55} & C_{56} \\ & & & & & C_{66} \end{bmatrix}. \tag{24}$$

According to Ting [26], the Stroh eigenvalues p_r and the eigenvectors $\boldsymbol{a}_r$ satisfy the following eigenrelation

$$\left[\boldsymbol{Q} + p\left(\boldsymbol{R} + \boldsymbol{R}^{\mathrm{T}}\right) + p^2\boldsymbol{T}\right]\boldsymbol{a} = 0, \tag{25}$$

where the superscript T denote the transpose of matrix, and $\boldsymbol{Q}$, $\boldsymbol{R}$, $\boldsymbol{T}$ are given by

$$\boldsymbol{Q} = \begin{bmatrix} C_{11} & C_{16} & C_{15} \\ C_{16} & C_{66} & C_{56} \\ C_{15} & C_{56} & C_{55} \end{bmatrix}, \quad \boldsymbol{R} = \begin{bmatrix} C_{16} & C_{12} & C_{14} \\ C_{66} & C_{26} & C_{46} \\ C_{56} & C_{25} & C_{45} \end{bmatrix},$$
$$\boldsymbol{T} = \begin{bmatrix} C_{66} & C_{26} & C_{46} \\ C_{26} & C_{22} & C_{24} \\ C_{46} & C_{24} & C_{44} \end{bmatrix}. \tag{26}$$

Due to $\boldsymbol{a} \neq \boldsymbol{0}$, p satisfies the sextic equation

$$\left|\boldsymbol{Q} + p\left(\boldsymbol{R} + \boldsymbol{R}^{\mathrm{T}}\right) + p^2\boldsymbol{T}\right| = 0. \tag{27}$$

According to Eq. (27), the solutions to the sextic equation are three pairs of complex conjugate roots for p. We take $\mathrm{Im}p_r > 0, r = 1, 2, 3$.

Introduce the matrix $\boldsymbol{N}$ and vector $\boldsymbol{b}$, and the expression of $\boldsymbol{N}$ is

$$\boldsymbol{N} = \begin{bmatrix} -\boldsymbol{T}^{-1}\boldsymbol{R}^{\mathrm{T}} & \boldsymbol{T}^{-1} \\ -\boldsymbol{Q} + \boldsymbol{R}\boldsymbol{T}^{-1}\boldsymbol{R}^{\mathrm{T}} & -\boldsymbol{R}\boldsymbol{T}^{-1} \end{bmatrix}. \tag{28}$$

Meanwhile, $\boldsymbol{p}$, $\boldsymbol{a}$, $\boldsymbol{b}$, and $\boldsymbol{N}$ satisfy the following relation

$$\boldsymbol{N}\begin{bmatrix} \boldsymbol{a}_r \\ \boldsymbol{b}_r \end{bmatrix} = p_r \begin{bmatrix} \boldsymbol{a}_r \\ \boldsymbol{b}_r \end{bmatrix} \quad r = 1, 2, 3, \tag{29}$$

$$\boldsymbol{b}_\alpha^{\mathrm{T}}\boldsymbol{a}_\beta + \boldsymbol{a}_\alpha^{\mathrm{T}}\boldsymbol{b}_\beta = \delta_{\alpha\beta}, \tag{30}$$

where $\delta_{\alpha\beta}$ is Kronecker delta.

Appendix 2

For the integral of Eq. (20), if the inclusion is rectangular, the contribution of each straight-line segment along the boundary of the inclusion can be obtained. We suppose the start point of certain straight-line segments is (x_1, y_1), and the end point is (x_2, y_2). As in Pan [25], the contribution of this straight-line segment along the boundary of the inclusion is

$$\begin{aligned}\varepsilon_{\beta\alpha} &= 0.5 n_i C_{ijlm} \varepsilon^{**}_{lm} \frac{l}{\pi} \mathrm{Im}\left\{\sum_{r=1}^{3} A_{jr} A_{\beta r} h_{r,\alpha}\right\} \\ &\quad + 0.5 n_i C_{ijlm} \varepsilon^{**}_{lm} \frac{l}{\pi} \mathrm{Im}\left\{\sum_{r=1}^{3} A_{jr} A_{\alpha r} h_{r,\beta}\right\}, \\ \varepsilon_{\alpha 3} &= 0.5 n_i C_{ijlm} \varepsilon^{**}_{lm} \frac{l}{\pi} \mathrm{Im}\left\{\sum_{r=1}^{3} A_{jr} A_{3r} h_{r,\alpha}\right\}, \end{aligned} \tag{31}$$

where $\alpha, \beta = 1, 2; r = 1, 2, 3; n_i$ is the outward normal component along the line segment: $n_1 = \frac{y_2 - y_1}{l}$, $n_2 = -\frac{x_2 - x_1}{l}$; $l = \sqrt{(x_2 - x_1)^2 + (y_2 - y_1)^2}$ is the length of the line segment; and $h_{r,1}$, $h_{r,2}$ are expressed as follows

$$\begin{aligned} h_{r,1} &= \frac{-1}{(x_2 - x_1) + p_r (y_2 - y_1)} \ln\left(\frac{x_2 + p_r y_2 - s_r}{x_1 + p_r y_1 - s_r}\right), \\ h_{r,2} &= \frac{-p_r}{(x_2 - x_1) + p_r (y_2 - y_1)} \ln\left(\frac{x_2 + p_r y_2 - s_r}{x_1 + p_r y_1 - s_r}\right). \end{aligned} \tag{32}$$

References

1. Nabarro, F.R.N.: Rafting in superalloy. Metall. Mater. Trans. A. **27**, 513–530 (1996)
2. Pollock, T.M., Argon, A.S.: Directional coarsening in nickel-base single crystals with high volume fractions of coherent precipitates. Acta Metall. Mater. **42**, 1859–1874 (1994)
3. Sakaguchi, M., Okazaki, M.: Fatigue life evaluation of a single crystal Ni-based superalloy, accompanying with change of microstructural morphology. Int. J. Fatigue. **29**, 1959–1965 (2007)
4. Tien, J.K., Copley, S.M.: The effect of uniaxial stress on the periodic morphology of coherent gamma prime precipitates in nickel-base superalloy crystals. Metall. Mater. Trans. B. **2**, 215–219 (1971)
5. Saito, M., Aoyama, T., Hidaka, K., et al.: Concentration profiles and the rafting mechanism of Ni base superalloys in the initial stage of high temperature creep tests. Scr. Mater. **34**, 1189–1194 (1996)
6. Zhang, Y., Wanderka, N., Schumacher, G., et al.: Phase chemistry of the superalloy SC16 after creep deformation. Acta Mater. **48**, 2787–2793 (2000)
7. Buffiere, J.Y., Ignat, M.: A dislocation based criterion for the raft formation in nickel-based superalloys single crystals. Acta Metall. Mater. **43**, 1791–1797 (1995)
8. Yue, Z.F., Lu, Z.Z., He, J.: Rafting prediction criterion for nickel-based single crystals under multiaxial stresses and crystallographic orientation dependence of creep behaviour. Acta Metall. Sin. **35**, 585–588 (1999). (in Chinese)
9. Kundin, J., Mushongera, L., Goehler, T., et al.: Phase-field modeling of the γ'-coarsening behavior in Ni-based superalloys. Acta Mater. **60**, 3758–3772 (2012)
10. le Graverend, J.B., Cormier, J., Gallerneau, F., et al.: A microstructure-sensitive constitutive modeling of the inelastic behavior of single crystal nickel-based superalloys at very high temperature. Int. J. Plastic. **59**, 55–83 (2014)
11. Socrate, S., Parks, D.M.: Numerical determination of the elastic driving force for directional coarsening in Ni-superalloys. Acta Metall. Mater. **41**, 2185–2209 (1993)
12. Müller, L., Glatzel, U., Feller-Kniepmeier, M.: Calculation of the internal stresses and strains in the microstructure of a single crystal nickel-base superalloy during creep. Acta Metall. Mater. **41**, 3401–3411 (1993)
13. Zhou, L., Li, S.X., Chen, C.R., et al.: Three-dimensional finite element analysis of stresses and energy density distributions around γ' before coarsening loaded in the [110]-direction in Ni-based superalloy. Mater. Sci. Eng. A. **352**, 300–307 (2003)
14. Pineau, A.: Influence of uniaxial stress on the morphology of coherent precipitates during coarsening-elastic energy considerations. Acta Metall. **24**, 559–564 (1976)
15. Chang, J.C., Allen, S.M.: Elastic energy changes accompanying the gamma- prime rafting in nickel-base superalloys. J. Mater. Res. **6**, 1843–1855 (1991)
16. Miyazaki, T., Nakamura, K., Mori, H.: Experimental and theoretical investigations on morphological changes of γ' precipitates in Ni-Al single crystals during uniaxial stress-annealing. J. Mater. Res. **14**, 1827–1837 (1979)
17. Ratel, N., Bruno, G., Bastie, P., et al.: Plastic strain-induced rafting of γ' precipitates in Ni superalloys: elasticity analysis. Acta Mater. **54**, 5087–5093 (2006)
18. Ratel, N., Bastie, P., Mori, T., et al.: Application of anisotropic inclusion theory to the energy evaluation for the matrix channel deformation and rafting geometry of $\gamma - \gamma'$ Ni Superalloys. Mater. Sci. Eng. A. **505**, 41–47 (2009)
19. Sakaguchi, M., Okazaki, M.: Micromechanics of the damage induced cellular microstructure in single crystal Ni-based superalloys. Acta Metall. Sin. **17**, 361–368 (2004)
20. Mori, T., Tanaka, K.: Average stress in matrix and average elastic energy of materials with misfitting inclusions. Acta Metall. **21**, 571–574 (1973)
21. Wu, W.P., Guo, Y.F., Dui, G.S., et al.: A micromechanical model for predicting the directional coarsening behavior in Ni-based superalloys. Comput. Mater. Sci. **44**, 259–264 (2008)
22. Chen, C.R., Li, S.X., Zhang, Q.: Finite element analysis of stresses associated with transformations in magnesia partially stabilized zirconia. Mater. Sci. Eng. A. **272**, 398–409 (1999)
23. Mura, T.: Micromechanics of Defects in Solids. Martinus Nijhoff, Leiden (1987)
24. Onaka, S., Kobayashi, N., Kato, M.: Two-dimensional analysis on elastic strain energy due to a uniformly eigenstrained supercircular inclusion in an elastically anisotropic material. Mech. Mater. **34**, 117–125 (2002)
25. Pan, E.: Eshelby problem of polygonal inclusions in anisotropic piezoelectric full- and half-planes. J. Mech. Phys. Solids. **52**, 567–589 (2004)
26. Ting, T.C.T.: Anisotropic Elasticity. Oxford University, Oxford (1996)